Applied Physics A (2018) 124:286
https://doi.org/10.1007/s00339-018-1717-z

Applied Physics A
Materials Science & Processing

Synthesis and properties of nickel-doped nanocrystalline barium hexaferrite ceramic materials

Moaz Waqar[1] · Muhammad Asif Rafiq[1] · Talha Ahmed Mirza[2] · Fazal Ahmad Khalid[1] · Abdul Khaliq[3] · Muhammad Sabieh Anwar[4] · Murtaza Saleem[4]

Received: 17 May 2017 / Accepted: 5 March 2018 / Published online: 9 March 2018

Abstract
M-type barium hexaferrite ceramics have emerged as important materials both for technological and commercial applications. However, limited work has been reported regarding the investigation of nanocrystalline Ni-doped barium hexaferrites. In this study, nanocrystalline barium hexaferrite ceramics with the composition $BaFe_{12-x}Ni_xO_{19}$ (where $x=0$, 0.3 and 0.5) were synthesized by sol–gel method and characterized using X-ray diffraction, Fourier transform infrared spectroscopy, scanning electron microscopy, vibrating sample magnetometer and precision impedance analyzer. All the synthesized samples had single magnetoplumbite phase having space group P63/mmc showing the successful substitution of Ni in $BaFe_{12}O_{19}$ without the formation of any impurity phase. Average grain size of undoped samples was around 120 nm which increased slightly with the addition of Ni. Saturation magnetization (M_s) and remnant magnetization (M_r) increased with the addition of Ni, however, coercivity (H_c) decreased with the increase in Ni from $x=0$ to $x=0.5$. Real and imaginary parts of permittivity decreased with the increasing frequency and increased with Ni content. Dielectric loss and conductivity showed slight variation with the increase in Ni concentration.

1 Introduction

Hexagonal ferrites (hexaferrites) have gained tremendous attention both technologically and commercially since their discovery in 1950s owing to their variety of applications in magnetic recording, ferrite cores, sensors, permanent magnets for power generation, loud speakers, small DC motors, microwave absorbers for microwave darkrooms, anti-electromagnetic interference coatings and in the fabrication of transistors, switch mode supplies and capacitors [1–8].

Hexaferrites have various types depending upon their structure including M, Z, Y, W, X and U. Among all these types, M-type hexaferrites specially $BaFe_{12}O_{19}$ (space group: P63/mmc) has attracted the interest of researchers in the recent years owing to their useful properties including large coercivity (594 kAm^{-1}), high magnetocrystalline anisotropy along c-axis (1352 kAm^{-1}), relatively large saturation magnetization (72 $Am^2\ kg^{-1}$), high electrical resistivity, chemical stability, high Curie temperature (450 °C), low cost, ability to resist corrosion, low eddy current and low dielectric losses [3, 9–13]. $BaFe_{12}O_{19}$ (BaM) has a large c-axis to a-axis ratio of 3.94 ($c=2.317$ nm and $a=0.589$ nm) which renders its large magnetocrystalline anisotropy [13]. A single molecular unit of BaM consists of two hexagonally packed (S) and two cubically packed (R) layers which are arranged in a sequence RSR* S* where S* and R* are 180° rotations of S and R, respectively. Fe^{3+} ions are responsible for magnetism in BaM. Each S block has 4 octahedral Fe^{3+} ions having 4 (spin up) moment and two tetrahedral Fe^{3+} ions having a 2 (spin down) moment, giving a net moment of 2 (spin up). Similarly, each R block has 3 (spin up), 2 (spin down) octahedral Fe^{3+} ions and 1 (spin up) Fe^{3+} ion at bipyramidal site giving a total net moment of 2 (spin up).

✉ Muhammad Asif Rafiq
asifrafiq@uet.edu.pk

[1] Department of Metallurgical and Materials Engineering, University of Engineering and Technology, G.T Road, Lahore 54890, Pakistan

[2] Department of Materials Science and Engineering, Friedrich-Alexander Universitat, Erlangen, Nurnberg, Germany

[3] Faculty of Science, Engineering and Technology, Swinburne University of Technology, Melbourne, Australia

[4] Department of Physics, Syed Babar Ali School of Science and Engineering, Lahore University of Management Sciences (LUMS), Opposite Sector U, D.H.A., Lahore 54792, Pakistan

So, S + R give a total moment of 4 (spin up) which equals 20 Bohr magnetrons (μ_B) [14].

Magnetic properties of BaM like saturation magnetization (M_s), remanent magnetization (M_r) and coercivity (H_c) can be modified/improved by several means including the substitution of Ba and/or Fe with various dopants/substituents [5, 9, 12, 15–18] and using different synthesis routes [13, 19–24]. Researchers have substituted Fe^{3+} with various trivalent ions [9, 16, 25] and a combination of divalent and tetravalent ions [11, 26, 27] to alter the properties of BaM. Different synthesis routes have also been employed to produce bulk and nanocrystalline BaM including solid state oxide route [8], hydrothermal method [28], glass crystallization method [21], microemulsion [20], co-precipitation [22], citrate precursor [19] and sol–gel auto-combustion method [29]. It has been observed that BaM having particle size ~ 100 nm show peculiar magnetic properties compared with those observed for sintered bulk materials [13, 19, 21, 23, 24].

Ni has been used as a dopant in combination with various tetravalent ions [18, 26, 27, 30–32] and has shown promising results, but a detailed investigation of solely Ni as a dopant in both bulk and nanocrystalline BaM is still scarce in literature. Recently, Rafiq et al. [8] studied the properties of bulk Ni-doped BaM ceramics and reported a good improvement in the magnetic properties. In the current study, effect of Ni^{2+} ions on the structural, magnetic and electric properties of nanocrystalline barium hexaferrites ($BaFe_{12}O_{19}$) prepared by sol–gel method has been investigated using advanced analytical techniques such as X-ray diffraction (XRD), Fourier transform infrared spectroscopy (FTIR), scanning electron microscopy (SEM), vibrating sample magnetometer (VSM) and precision impedance analyzer. Impedance analysis has emerged as an important modern technique to investigate the electrical properties of ceramics. Therefore, a detailed dielectric study has been done to characterize the dielectric properties of samples using precision impedance analyzer in the frequency range from 1 kHz to 2 MHz. The frequency range from kHz to MHz is the most common frequency range, in which data is normally reported to study the various possibilities of electric polarization [8, 33, 34]. A relationship between structure/microstructure and magnetic and electric properties has been established which will be helpful in optimizing the properties of these ceramics for commercial applications.

2 Experimental

Ni-substituted barium hexaferrites with formula $BaFe_{12-x}Ni_xO_{19}$ where $x = 0$, 0.3 and 0.5 were synthesized using sol–gel method. Stoichiometric ratios of $Fe(NO_3)_3{\cdot}9H_2O$ (Sigma Aldrich, 99%), $Ba(NO_3)_2$ (Sigma Aldrich, 99%) and $Ni(NO_3)_2.6H_2O$ (Sigma Aldrich, 99%) were dissolved in 50 ml of distilled water. Citric acid ($C_6H_8O_7{\cdot}H_2O$) (Sigma Aldrich, 99%) solution was added to the solution obtained in previous step according to molar ratio of 1:1 (citric acid/metal ions) for the chelation of Ba^{2+}, Fe^{3+} and Ni^{2+} ions. As a result, a clear aqueous solution with a pH value of 7 was obtained by adjusting it with NH_4OH. This neutralized solution was water bathed at 80 °C for 4 h and was continuously stirred to complete the reaction. After the evaporation of water, a brown viscous wet gel was obtained which was dried in oven at 150 °C for 24 h and as a result gel was formed. This dry gel was pre-heated at 450 °C for 2 h and then calcined at 900 °C for 4 h to obtain the desired pure phase. Crystallographic properties of the synthesized samples were studied using X-ray diffractometer (PANalytical Xpert PRO) with Cu–Kα ($\lambda = 0.154$ nm) radiation. Fourier transform infrared (Jasco FT/IR-4100) spectrometer was used to perform infrared spectroscopic analysis of the samples in the range of 400–1600 cm^{-1} with a resolution of 4 cm^{-1}. Scanning electron microscope (Nova NanoSEM 450) was used to analyze particle size and morphological aspects of the samples. Vibrating sample magnetometer (Model: 7407, Lakeshore (USA)) was used to plot magnetic hysteresis curves at room temperature. Dielectric properties of the samples were analyzed using precision impedance analyzer (Wayne kerr 6500B) over the frequency range of 1 kHz–2 MHz at room temperature.

3 Results and discussion

The structure and purity of undoped and doped nanocrystalline barium hexaferrite ceramics were investigated using XRD and the resultant patterns have been shown in Fig. 1. All the peaks are indexed in accordance with joint committee on powder diffraction standard (JCPDS) no. 84–0757 and the standard pattern has also been presented at the base of Fig. 1 as a reference. The results clearly show the formation of hexagonal magnetoplumbite structure having space group P63/mmc in all the samples. The doped Ni successfully substituted Fe in the crystal lattice of BaM and no secondary phase was formed even at higher level of substitution, i.e., at $x = 0.5$. Lattice parameters a and c were calculated according to the formula [11].

$$\frac{1}{d_{hkl}^2} = \frac{4\,(h^2 + hk + k^2)}{3a^2} + \frac{l^2}{c^2}. \quad (1)$$

Where h, k and l are miller indices, and d is the interplanar spacing determined by Bragg's Law which is $n\lambda = 2d\sin\theta$. The unit cell volume V_{cell} was calculated from the formula [11].

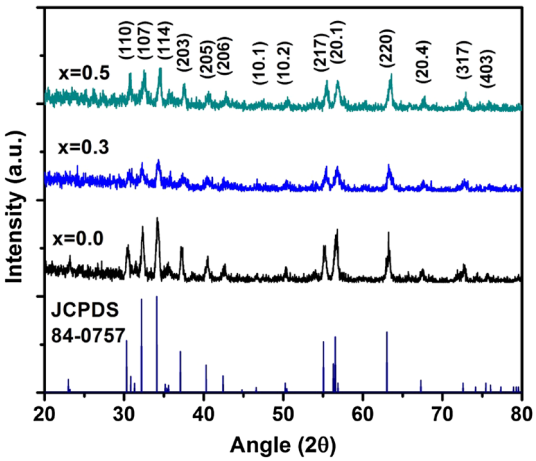

Fig. 1 XRD patterns for $BaFe_{12-x}Ni_xO_{19}$ for increasing values of x. Hexagonal magnetoplumbite structure (space group: P63/mmc) was formed in all the samples without the formation of any secondary phase

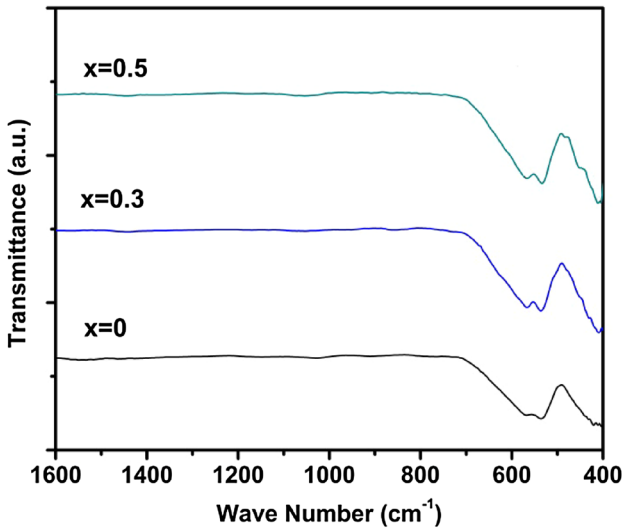

Fig. 2 FTIR spectra of $BaFe_{12-x}Ni_xO_{19}$ for $x=0$, 0.3 and 0.5. Only metal–oxygen ions were observed indicating the formation of hexaferrites

$$V_{cell} = \frac{\sqrt{3}}{2}a^2c. \quad (2)$$

The results have been shown in Table 1. The observed values of lattice parameters for undoped BaM ($a=0.5884$ nm, $c=2.3007$ nm) are in good agreement with the previous investigations [9, 10]. It is evident from Table 1 that there was an increase in the length of c-axis with the increasing amount of Ni which can be explained on the basis of larger ionic radius of Ni^{2+} ions ($r(Ni^{2+})=0.069$ nm with coordination number (CN) = 4 and $r(Ni^{2+})=0.083$ nm for CN = 6) [35] which are replacing smaller Fe^{3+} ions ($r(Fe^{3+})=0.063$ nm with CN = 4 and $r(Fe^{3+})=0.0785$ nm with CN = 6 [35]) in the hexagonal crystal lattice [36]. There is a linear increase in the c/a ratio which is expected to effect the magnetocrystalline anisotropy of the crystals [13, 32].

Figure 2 shows the Fourier transformed infrared (FTIR) spectroscopy results of nanocrystalline $BaFe_{12-x}Ni_xO_{19}$ (where $x=0$, 0.3 and 0.5) ceramics recorded at room temperature in the range 400–1600 cm^{-1}. Two strong absorption peaks in the range of 400 and 800 cm^{-1} were observed from FTIR spectra. These characteristic absorption bands can be related to the stretching vibration of Fe–O molecule in octahedral and tetrahedral sites [4, 37]. Two absorption peaks can be seen in the range 550–580 cm^{-1} and 430–470 cm^{-1}. These peaks were assigned to the vibration of the bond between the oxygen ion and the tetrahedral metal-ion (O–M tetra) and octahedral metal-ion (O–M octa), respectively [9]. It can also be seen that the peaks are gradually shifting towards low frequency side with increasing Ni^{+2} content. This shifting can be attributed to the substitution of large Ni^{+2} ions affecting the distribution of Fe^{+3} ions [4]. Moreover, the change in the band position can also be attributed to the change in the Fe^{+3}–O^{-2} intermolecular distances for tetrahedral and octahedral sites [38].

Table 1 Values of lattice constants 'a' and 'c', c/a ratio and volume of unit cell of $BaFe_{12-x}Ni_xO_{19}$

Composition	a (nm)	c (nm)	c/a	V_{cell} $(nm)^3$
$BaFe_{12}O_{19}$	0.5884	2.3007	3.910	0.6898
$BaFe_{11.7}Ni_{0.3}O_{19}$	0.5876	2.3175	3.942	0.6931
$BaFe_{11.5}Ni_{0.5}O_{19}$	0.5858	2.3301	3.977	0.6926

To confirm the grain size and to investigate the morphological aspects of $BaFe_{12-x}Ni_xO_{19}$ ($x=0$, 0.3 and 0.5) ceramic samples, SEM was done and results have been shown in Fig. 3. SEM image of calcined $BaFe_{12}O_{19}$ powder has been shown in Fig. 3a, which confirms the nanocrystalline nature of the samples with an average grain size of ~ 105 nm. Figure 3b, c and d show the SEM micrographs of $BaFe_{12-x}Ni_xO_{19}$ ($x=0$, 0.3 and 0.5) sintered ceramics. A slight increase in the average grain size of ceramics from ~ 121 to ~ 131 nm was observed with increasing amount of Ni from $x=0$ to $x=0.5$, respectively. Average particles sizes are presented in Table 2. This small increase in grain size can be attributed to the formation of oxygen vacancies, as it is already know from literature that diffusion of vacancies during sintering plays a vital role in grain growth of the ceramics [8, 39].

To analyze the magnetic properties of the samples, vibrating sample magnetometry (VSM) was done. The M–H hysteresis curve for nanocrystalline $BaFe_{1212-x}Ni_xO_{19}$ ($x=0$, 0.3 and 0.5) ceramics are displayed in Fig. 4 and corresponding values of M_s, M_r, and H_c are tabulated in Table 2.

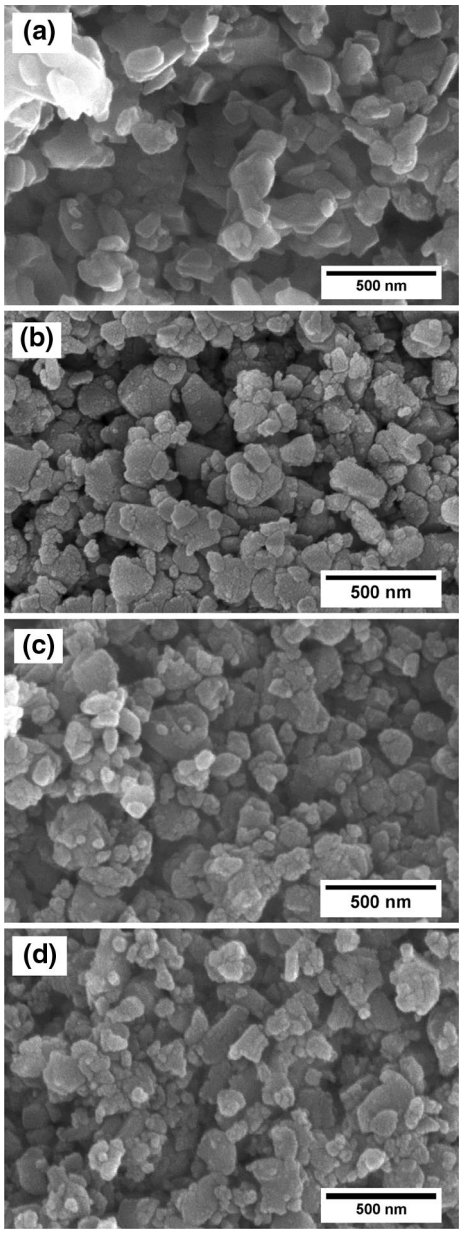

Fig. 3 **a** SEM image of non-sintered and undoped $BaFe_{12}O_{19}$, to confirm the formation of nano-sized powder. SEM images of sintered $BaFe_{12-x}Ni_xO_{19}$ ceramics for **b** $x=0$, **c** $x=0.3$ and **d** $x=0.5$. There is a slight increase in grain size with the addition of Ni

An increase in saturation magnetization (M_s) was observed with the increasing amount of Ni^{2+}. This behavior can be attributed to the increase in net magnetic polarization of $BaFe_{12-x}Ni_xO_{19}$ due to the substitution of Ni and it can be explained as follows: Ligand field theory states that ions with d^1, d^2, d^3 and d^4 electrons prefer tetrahedral coordination, while ions with d^6, d^7, d^8 and d^9 electrons prefer octahedral coordination [8, 30, 40]. Furthermore, it is known from the literature that Ni^{2+} has a site preference energy of around 20 kcal/mol for symmetrical octahedral site which is higher than the energy required to occupy tetrahedral site, which in turn makes octahedral site occupancy more suitable for Ni^{2+} ions [27]. Both arguments support the fact that Ni^{+2} ions are expected to replace Fe^{+3} ions at 2a (Spin Up) and $4f^2$ (Spin down) for small values of substitution. Now, net magnetic polarization (J) at any temperature T per unit formula of BaM can be given by [8, 26].

$$J(T) = 6m_{12k}(T) - 2m_{4f1}(T) - 2m_{4f2}(T) + 1m_{2a}(T) + 1m_{2b}(T) \quad (3)$$

where m_n is the magnetic moment of Fe^{3+} ions in the nth sub-lattice. The increase in M_s with increasing amount of x suggests that Ni^{2+} ions ($3\mu_B$) have preferentially replaced Fe^{3+} ions ($5\mu_B$) at $4f^2$, which resulted in the increase of net magnetic moment per unit formula from $20\mu_B$ to $22\mu_B$ according to Eq. 3 which consequently resulted in the increase of M_s. These results are in accordance with the Mossbauer studies of Ni–Zr doped barium hexaferrites [40]. Remnant magnetization also showed an increasing trend with the increase in Ni concentration. Coercivity showed little variation on increasing the amount of Ni from $x=0$ to $x=0.3$, but with the further increase to $x=0.5$, the coercivity dropped drastically. This decrease in coercivity can be attributed to the decrease in magnetocrystalline anisotropy of Ni-doped barium hexaferrites. It is reported that Ni is effective in decreasing the magnetocrystalline anisotropy of BaM and the rate of decrease of magnetocrystalline anisotropy is directly proportional to the Ni content [27].

The dielectric properties of $BaFe_{12-x}Ni_xO_{19}$ were measured over a frequency range of 1 kHz to 2 MHz at room temperature and the results are shown in Fig. 5. The variation of real and imaginary part of complex permittivity (ε' and ε'') with frequency is shown in Fig. 5a, b. The energy

Table 2 Effect of dopant on the magnetic properties and grain size of nanocrystalline $BaFe_{12-x}Ni_xO_{19}$ ceramics for $x=0$, 0.3 and 0.5

Composition	Saturation magnetization M_s emu/g	Remanent magnetization M_r emu/g	Coercivity H_c Oe	Average grain size d nm
$BaFe_{12}O_{19}$ (non-sintered)	–	–	–	105.02
$BaFe_{12}O_{19}$	21.41	12.32	2928.7	121.05
$BaFe_{11.7}Ni_{0.3}O_{19}$	23.43	12.96	2984.4	129.43
$BaFe_{11.5}Ni_{0.5}O_{19}$	26.06	14.14	1738.9	131.03

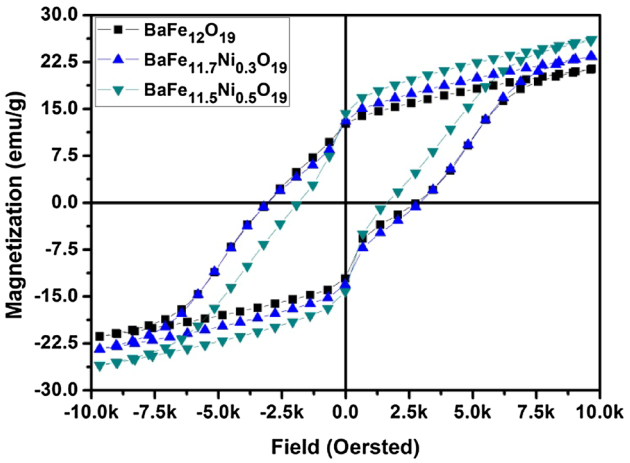

Fig. 4 M–H loops for nanocrystalline $BaFe_{12-x}Ni_xO_{19}$ ceramics for $x = 0$, 0.3 and 0.5

stored in the dielectric material due to alternating current (AC) field is a function of its permittivity and is represented by the real part of permittivity (ε'), whereas the imaginary part (ε'') represents the losses [9]. As seen in Fig. 5a, b, the real part of permittivity (ε') and the imaginary part (ε'') showed a decreasing trend with the increase in frequency for all the compositions in the measured frequency range. This trend can be attributed to the decrease in polarization with the increase in frequency and can be explained as follows; the total or net polarization for a dielectric material is the sum of contributions from ionic, electronic, dipolar and interfacial polarizations [41–44]. At low frequency, all of these polarizations are quite responsive to the time varying electric field, but as the frequency of this electric field is increased, the contributions from different polarization filter out which result in the decrease of net polarization. Consequently, permittivity of the ceramic decreases [34, 42, 43]. Second, ferrites are known to have grains with good conductance, whereas grain boundaries are highly resistive in nature. On the application of electric field, electrons tend to move towards the grain boundary favorably through hopping mechanism and start accumulating due to the high resistance of grain boundary which causes polarization. When the frequency of the applied electric field is increased, the frequency of electrons changing their direction of motion increases as well. This phenomenon decreases the probability of electrons to reach the grain boundary and as a result of this, polarization decreases. Consequently, the dielectric constant decreases with the increase in frequency of applied electric field. The results obtained in the present work are in accordance with previous reports [41, 43, 45]. It can also be seen in Fig. 5a, b that the real part of permittivity (ε') and imaginary part (ε'') increased with the increase in Ni content. It can be explained by the mechanism of electron hopping in ferrites. In ferrites, conduction takes place by

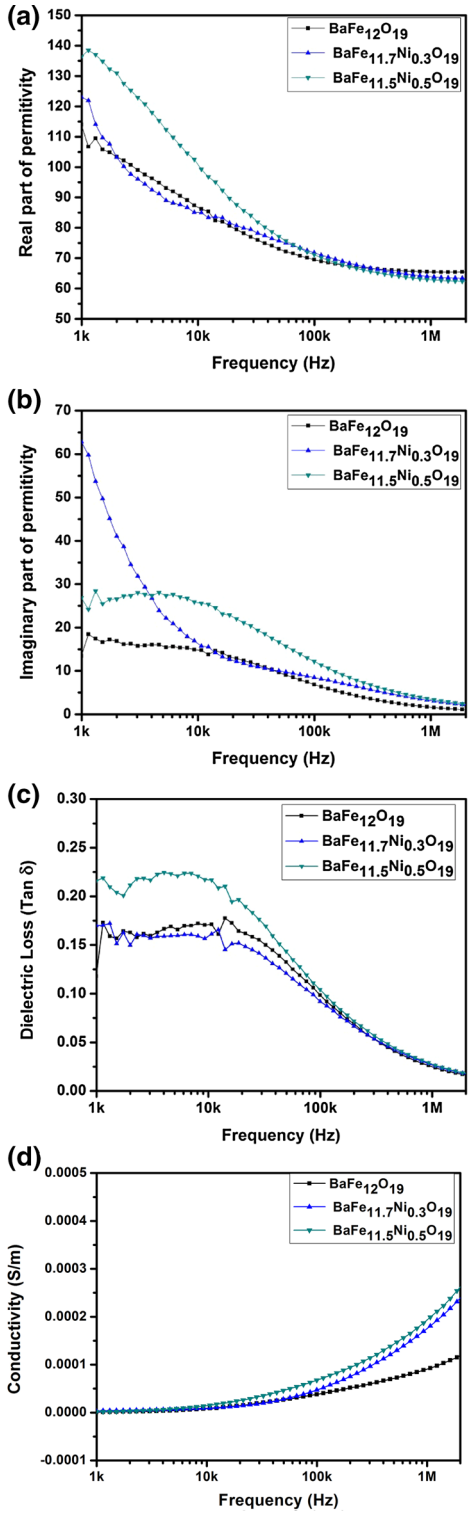

Fig. 5 Effect of frequency on **a** Real part of permittivity. **b** Imaginary part of permittivity. **c** Dielectric loss and **d** conductivity of $BaFe_{12-x}Ni_xO_{19}$ for $x = 0$, 0.3 and 0.5

hopping of electrons between ions which are present in more than one valence state distributed randomly among crystallographic lattice sites. So, hopping of electrons between Fe^{2+} and Fe^{3+} ions is the prime mode of conduction. As already discussed, the electrons reach the grain boundary by hopping mechanism, and due to it high resistivity, they get piled up and thereby produce space charge polarization [43]. By the addition of divalent Ni ions, the exchange interaction between Ni^{2+} and Fe^{3+} may become possible resulting in the conversion of Fe^{3+} into Fe^{2+} and Ni^{2+} into Ni^{3+} ions. This interaction might contribute to the increase in electron/hole hopping between Fe^{3+} and Fe^{2+} as well as between Ni^{3+} and Ni^{2+} ions which in turn increases the piling up of electrons at the grain boundary. Hence increase in the buildup of space charge polarization might have decreased the values of ε' and ε'' [15].

Figure 5c indicates the variation of tan δ with frequency for $BaFe_{12-x}Ni_xO_{19}$ ceramics (where $x=0$, 0.3 and 0.5). The value of dielectric loss varied between 0.10 and 0.25 for all the compositions at lower frequency. Further decrease in dielectric loss was observed with the increase in frequency. This decrease can be due to the fact that the dipole oscillations cannot follow the changes of the external field at high frequencies [46]. Figure 5d indicates the variation of conductivity with increasing frequency for all the compositions. There was a small increase in conductivity with increasing frequency in the measured frequency range. The mechanism of conduction in hexaferrites has already been explained. The increase in conductivity at higher frequency is attributed to the increased mobility of charge carriers. At low frequency, grain boundaries behave as active medium which impart high resistance to charge carriers and which explains the low conductivity at lower frequency. At high frequency, grains behave as active medium which results in a decrease in resistance. Moreover, there might be an increase in electrons hopping among Fe^{3+} and Fe^{2+} ions, which might have attributed to the increase in the conductivity at higher frequency [33, 47, 48]. Further work is required to fully understand this mechanism and work in this direction is also being carried out using the impedance spectroscopic technique and complete results will be published elsewhere.

4 Conclusion

Ni-substituted nanocrystalline barium hexaferrite samples have been successfully synthesized using sol–gel method. X-ray diffraction analysis revealed the formation of hexagonal magnetoplumbite structure (space group P63/mmc) in all the samples without the formation of secondary phase. SEM images confirmed the formation of nano-sized powder and average grain size showed very small variation, i.e., from 121 to 131 nm with the increase in Ni content from $x=0$ to $x=0.5$. Saturation magnetization (M_s) and remnant magnetization (M_r) increased with the addition of Ni from 21.41 to 26.6 emu/g and 12.32 to 14.14 emu/g, respectively; however, coercivity (H_c) decreased from 2928.7 Oe to 1738.9 Oe with the increase in Ni from $x=0$ to $x=0.5$. Real and imaginary part of permittivity decreased with the increasing frequency and increased with Ni content. Dielectric loss varied between 0.03 and 0.25 in the measured frequency range and conductivity showed slight variation with the increase in dopant concentration.

Compliance with ethical standards

Conflict of interest The authors declare that they have no conflict of interest.

References

1. T. Kaur et al., Effect on dielectric, magnetic, optical and structural properties of Nd–Co substituted barium hexaferrite nanoparticles. Appl. Phys. A **119**(4), 1531–1540 (2015)
2. J. Li et al., Phase formation, magnetic properties and Raman spectra of Co–Ti co-substitution M-type barium ferrites. Appl. Phys. A **119**(2), 525–532 (2015)
3. V.N. Dhage et al., Structural and magnetic behaviour of aluminium doped barium hexaferrite nanoparticles synthesized by solution combustion technique. Phys. B **406**(4), 789–793 (2011)
4. Chavan, V.C., et al., Transformation of hexagonal to mixed spinel crystal structure and magnetic properties of Co_{2+} substituted $BaFe_{12}O_{19}$. J. Magnet. Magnet. Mater.. **398**, 32–37 (2016)
5. V.N. Dhage et al., Influence of chromium substitution on structural and magnetic properties of $BaFe_{12}O_{19}$ powder prepared by sol–gel auto combustion method. J. Alloy. Compd. **509**(12), 4394–4398 (2011)
6. Z. Zhang et al., Effect of Nd–Co substitution on magnetic and microwave absorption properties of SrFe $_{12}O_{19}$ hexaferrites. J. Alloy. Compd. **525**, 114–119 (2012)
7. X. Niu et al., Effects of presintering temperature on structural and magnetic properties of $BaMg_{1.8}Cu_{0.2}Fe_{16}O_{27}$ hexagonal ferrites. Optics **126**(24), 5513–5516 (2015)
8. M.A. Rafiq et al., Effect of Ni^{2+} substitution on the structural, magnetic, and dielectric properties of barium hexagonal ferrites ($BaFe_{12}O_{19}$). J. Electron. Mater. 46(1), 241–246 (2017)
9. Z. Mosleh et al., Structural, magnetic and microwave absorption properties of Ce-doped barium hexaferrite. J. Magn. Magn. Mater. **397**, 101–107 (2016)
10. L. Wang et al., XAFS and XPS studies on site occupation of Sm^{3+} ions in Sm doped M-type $BaFe_{12}O_{19}$. J. Magn. Magn. Mater. **377**, 362–367 (2015)
11. M.H. Shams et al., Effect of Mg^{2+} and Ti^{4+} dopants on the structural, magnetic and high-frequency ferromagnetic properties of barium hexaferrite. J. Magn. Magn. Mater. **399**, 10–18 (2016)
12. G.M. Rai, M. Iqbal, K. Kubra, Effect of Ho^{3+} substitutions on the structural and magnetic properties of $BaFe_{12}O_{19}$ hexaferrites. J. Alloy. Compd. **495**(1), 229–233 (2010)
13. R.C. Pullar, Hexagonal ferrites: a review of the synthesis, properties and applications of hexaferrite ceramics. Prog. Mater Sci. **57**(7), 1191–1334 (2012)
14. J. Smit, H.P.J. Wijn, *Ferrites*. Philips Technical Library, Eindhoven, 1959

15. M.J. Iqbal, S. Farooq, Suitability of $Sr_{0.5}Ba_{0.5-x}Ce_xFe_{12-y}Ni_yO_{19}$ co-precipitated nanomaterials for inductor applications. J. Alloys Compd. **493**(1–2), 595–600 (2010)
16. C.-J. Li, B. Wang, J.-N. Wang, Magnetic and microwave absorbing properties of electrospun $Ba_{(1-x)}La_xFe_{12}O_{19}$ nanofibers. J. Magn. Magn. Mater. **324**(7), 1305–1311 (2012)
17. I. Bsoul, S. Mahmood, Magnetic and structural properties of $BaFe_{12-x}Ga_xO_{19}$ nanoparticles. J. Alloy. Compd. **489**(1), 110–114 (2010)
18. S. Singhal, A. Garg, K. Chandra, Evolution of the magnetic properties during the thermal treatment of nanosize $BaMFe_{11}O_{19}$ (M = Fe, Co, Ni and Al) obtained through aerosol route. J. Magn. Magn. Mater. **285**(1), 193–198 (2005)
19. V. Sankaranarayanan, D. Khan, Mechanism of the formation of nanoscale M-type barium hexaferrite in the citrate precursor method. J. Magnet. Magnet. Mater. **153**(3), 337–346 (1996)
20. X. Liu et al., An ultrafine barium ferrite powder of high coercivity from water-in-oil microemulsion. J. Magn. Magn. Mater. **184**(3), 344–354 (1998)
21. L. Rezlescu et al., Fine barium hexaferrite powder prepared by the crystallisation of glass. J. Magn. Magn. Mater. **193**(1), 288–290 (1999)
22. A. Ataie, S. Heshmati-Manesh, Synthesis of ultra-fine particles of strontium hexaferrite by a modified co-precipitation method. J. Eur. Ceram. Soc. **21**(10), 1951–1955 (2001)
23. M. Iqbal, A. Mir, S. Alam, Synthesis and characterizations of nano-sized barium hexa ferrites using sol-gel methods. une **13**, 15 (2016)
24. A. Mali, A. Ataie, Structural characterization of nano-crystalline $BaFe_{12}O_{19}$ powders synthesized by sol–gel combustion route. Scripta Mater. **53**(9), 1065–1070 (2005)
25. D. Chen et al., Curie temperature and magnetic properties of aluminum doped barium ferrite particles prepared by ball mill method. J. Magn. Magn. Mater. **395**, 350–353 (2015)
26. H. Sözeri et al., Magnetic, dielectric and microwave properties of M–Ti substituted barium hexaferrites (M = Mn^{2+}, Co^{2+}, Cu^{2+}, Ni^{2+}, Zn^{2+}). Ceram. Int. **40**(6), 8645–8657 (2014)
27. M.V. Rane et al., Magnetic properties of NiZr substituted barium ferrite. J. Magn. Magn. Mater. **195**(2), L256–L260 (1999)
28. D. Mishra et al., Studies on characterization, microstructures and magnetic properties of nano-size barium hexa-ferrite prepared through a hydrothermal precipitation–calcination route. Mater. Chem. Phys. **86**(1), 132–136 (2004)
29. L. Junliang et al., Synthesis and magnetic properties of quasi-single domain M-type barium hexaferrite powders via sol–gel auto-combustion: Effects of pH and the ratio of citric acid to metal ions (CA/M). J. Alloy. Compd. **479**(1), 863–869 (2009)
30. A. Gonzalez-Angeles et al., Magnetic studies of NiSn-substituted barium hexaferrites processed by attrition milling. J. Magn. Magn. Mater. **270**(1), 77–83 (2004)
31. P. Meng et al., Tunable complex permeability and enhanced microwave absorption properties of $BaNi_xCo_{1-x}TiFe_{10}O_{19}$. J. Alloy. Compd. **628**, 75–80 (2015)
32. D. Vinnik et al., Growth, structural and magnetic characterization of Co-and Ni-substituted barium hexaferrite single crystals. J. Alloy. Compd. **628**, 480–484 (2015)
33. Q.K. Muhammad et al., Structural, dielectric, and impedance study of ZnO-doped barium zirconium titanate (BZT) ceramics. J. Mater. Sci. 1–11 (2016)
34. A. Kamal et al., Structural and impedance spectroscopic studies of CuO-doped ($K_{0.5}Na_{0.5}Nb_{0.995}Mn_{0.005}O_3$) lead-free piezoelectric ceramics. Appl. Phys. A **122**, 1037 (2016)
35. R.D. Shannon, Revised effective ionic radii and systematic studies of interatomic distances in halides and chalcogenides. Acta Crystallogr. Sect. A **32**(5), 751–767 (1976)
36. P.P. Naik et al., Influence of rare earth (Nd^{+3}) doping on structural and magnetic properties of nanocrystalline manganese-zinc ferrite. Mater. Chem. Phys. (2017)
37. R.S. Alam et al., Structural, magnetic and microwave absorption properties of doped Ba-hexaferrite nanoparticles synthesized by co-precipitation method. J. Magn. Magn. Mater. **381**, 1–9 (2015)
38. M. Rasly, M.M. Rashad, Structural and magnetic properties of Sn–Zn doped $BaCo_2$ Z-type hexaferrite powders prepared by citrate precursor method. J. Magn. Magn. Mater. **337–338**, 58–64 (2013)
39. I. Coondoo et al., Structural, dielectric and impedance spectroscopy studies in $(Bi_{0.90}R_{0.10})Fe_{0.95}Sc_{0.05}O_3$. [R = La, Nd] ceramics. Ceram. Int. **40**(7), 9895–9902 (2014)
40. M.V. Rane et al., Mössbauer and FT-IR studies on non-stoichiometric barium hexaferrites. J. Magn. Magn. Mater. **192**(2), 288–296 (1999)
41. A.K. Singh et al., Dielectric properties of Mn-substituted Ni–Zn ferrites. J. Appl. Phys. **91**(10), 6626–6629 (2002)
42. M.A. Rafiq, M.N. Rafiq, K.V. Saravanan, Dielectric and impedance spectroscopic studies of lead-free barium-calcium-zirconium-titanium oxide ceramics. Ceram. Int. **41**(9), 11436–11444 (2015)
43. I. Soibam, S. Phanjoubam, L. Radhapiyari, Dielectric properties of Ni substituted Li–Zn ferrites. Phys. B **405**(9), 2181–2184 (2010)
44. M.A. Rafiq et al., Defects and charge transport in Mn-doped $K_{0.5}Na_{0.5}NbO_3$ ceramics. Phys. Chem. Chem. Phys. **17**(37), 24403–24411 (2015)
45. M.A. Rafiq et al., Impedance analysis and conduction mechanisms of lead free potassium sodium niobate (KNN) single crystals and polycrystals: a comparison study. Cryst. Growth Des. **15**(3), 1289–1294 (2015)
46. V.V. Soman et al., Effect of substitution of Zn-Ti on magnetic and dielectric properties of $BaFe_{12}O_{19}$. Phys. Proc. **54**, 30–37 (2014)
47. S. El-Sayed et al., Magnetic behavior and dielectric properties of aluminum substituted M-type barium hexaferrite. Phys. B **426**, 137–143 (2013)
48. V.V. Soman, V. Nanoti, D. Kulkarni, Dielectric and magnetic properties of Mg–Ti substituted barium hexaferrite. Ceram. Int. **39**(5), 5713–5723 (2013)